Predicting enhanced mass flow rates in gas microchannels using nonkinetic models

Dadzie, Kokou Sename Enyonam; Brenner, Howard

Published in:
Physical Review E

DOI:
10.1103/PhysRevE.86.036318

Publication date:
2012

Predicting enhanced mass flow rates in gas microchannels using nonkinetic models

S. Kokou Dadzie[*]
Mechanical and Aeronautical Engineering, Glyndŵr University, Mold Road, Wrexham LL11 2AW, UK

Howard Brenner[†]
Department of Chemical Engineering, Massachusetts Institute of Technology, Cambridge, Massachusetts 02139-4307, USA
(Received 21 May 2012; published 21 September 2012)

Different nonkinetic approaches are adopted in this paper towards theoretically predicting the experimentally observed phenomenon of enhanced mass flow rates accompanying pressure-driven rarefied gas flows through microchannels. Our analysis utilizes a full set of mechanically consistent volume-diffusion hydrodynamic equations, allowing complete, closed-form, analytical solutions to this class of problems. As an integral part of the analysis, existing experimental data pertaining to the subatmospheric pressure dependence of viscosity were analyzed. The several nonkinetic approaches investigated were (1) pressure-dependent viscosity exponent model, (2) slip-velocity models, and (3) volume diffusion model. We explored the ability to predict the gas's mass flow rate over the full range of Knudsen numbers, including furnishing a physically sound interpretation of the well-known Knudsen minimum observed in the mass flow rate. Matching of a pressure-dependent viscosity model, one that follows the standard temperature-viscosity power law and its supporting single momentum diffusion mechanism, did not allow an accurate interpretation of the data. Rather, matching of this model with the flow rate was found to mismatch the experimental pressure dependence of the viscosity. An additional transport mechanism model, one based on volume diffusion, offered a comprehensive understanding of the Knudsen minimum, while also resulting in excellent agreement with experimental data well into the transition regime (up to a Knudsen number of 5).

DOI: 10.1103/PhysRevE.86.036318 PACS number(s): 47.61.−k, 47.40.−x, 47.45.−n

I. INTRODUCTION

Expanding demands in microdevice technology involving the motion of fluids at micro- and nanolength scales open a new branch in fluid mechanics requiring investigation of fluid flows occurring exclusively in ultrasmall devices. Examples of these mechanical systems include micropumps, heat exchangers, jet polishing and cutting systems, and, more importantly, the entire range of micro-electro-mechanical systems encompassing their various bioengineering applications [1–3].

Knudsen [4] was the first to report data pointing to the anomalous behavior of gases flowing in microchannels. Many experiments have since confirmed Knudsen's initial observations. Among these are experiments conducted by Porodonov *et al*. [5], Arkilic *et al*. [6], Maurer *et al*. [7], and Ewart *et al*. [8]. Comprehensive experimental data concerning other important flow parameters, such as streamwise and lateral pressure, velocity, and temperature distributions in this domain, are, however, still lacking. Anomalies, such as Knudsen's minimum in the mass flow rate during pressure-driven flows, are interpreted as constituting deviations from equilibrium associated with high Knudsen numbers [2,3], and classified accordingly in the kinetic theory of gases.

In regard to theoretical modeling of these anomalies, it is now widely accepted that the standard set of fluid mechanical equations, namely, those due to Navier-Stokes-Fourier, are inapplicable. In their stead, Boltzmann's kinetic equation for dilute gases constitutes the present standard kinetic model when addressing nonequilibrium gas flows [9,10]. The numerical simulation of the BGK kinetic equation performed by Sharipov [11] is frequently cited as offering the best fit with experimental data [8,11]. On the other hand, it has been noted since the celebrated work of Maxwell [12] that a simple adjustment of the tangential-velocity boundary condition at a solid boundary, allowing for slip rather than adherence, can improve the agreement between Navier-Stokes and experiments.

A major advantage of analytical methods over kinetic approaches and other numerical methods lies in their ultimate ability to allow convenient interpretations and straightforward tracking of all physical parameters involved in the modeling. As such, significant attempts have been made to extend and improve Maxwell's introduction of slip boundary conditions in order to predict anomalous phenomena such as those observed in Knudsen's experiments. Among these is a series of attempts to extend slip boundary conditions so as to include higher-order terms [2,3,13,14]. The use of first-order slip boundary conditions is subject to an uncertainty as to the value of the phenomenological coefficient appearing therein, particularly Maxwell's accommodation coefficient. Second- and higher-order slip conditions are, however, criticized for being incompatible with the order of the continuum flow differential equations. Other attempts have focused on modeling the slip coefficient itself. Following this, a variable mean-free path model was introduced by Arlemark *et al*. [15], although the improvement achieved in enhancing accord with experimental data did not markedly exceed that for the traditional slip cases. Dongari *et al*. [16], combined this approach with a description wherein the total mass flux through the channel is regarded as composed of a combination of convective and diffusive fluxes.

[*]k.dadzie@glyndwr.ac.uk
[†]hbrenner@mit.edu

Their scheme resulted in reasonably good agreement with data over the full Knudsen number range. However, the value of the Knudsen minimum was underpredicted.

Gallis and Torczynski [17], using a direct simulation Monte Carlo (DSMC) scheme, simulated gas flowing through microtubes. To match their simulations with experimental data they introduced a total of four extra fitting parameters. The need for this large number of parameters may be viewed as indicative of a failure of that approach to provide physically sound interpretations of those experiments. Zhang *et al.* [18] and Michalis *et al.* [19] used the DSMC method to investigate the respective successes of the effective diffusion coefficient and effective viscosity laws for noncontinuum flow predictions. The changeover to effective transport coefficients demonstrates the existence of differences in the respective mechanisms of mass and momentum transport between the respective slip-transition and pure continuum regimes.

Gorji *et al.* [20] obtained the mass flow rate by solving, numerically, a velocity-space stochastic equation addressing molecular motions. Following this they proposed a kinetic model involving replacement of the Boltzmann collision integral operator by a velocity-space diffusion operator. This led to a Fokker-Planck stochastic kinetic equation, whose solution they reported to agree with data up to a Knudsen number of 5 for gaseous argon [20,21]. The experimental data used in the comparison were those of Dong [22].

The preceding Fokker-Planck kinetic equation presented by Gorji *et al.* [20] possesses an intrinsic link to the class of so-called volume-mass diffusion or bivelocity hydrodynamic models that have appeared recently [23–27]. Indeed, the exact Fokker-Planck stochastic equation had previously been proposed and investigated by Bogomolov and Dorodnitsyn [23]. Using an appropriate stochastic integration of the same stochastic kinetic equation addressing molecular motions, Bogomolov and Dorodnitsyn derived a hydrodynamic equation wherein a diffuse flux term involving the mass-density gradient appears in the set of macroscopic continuum equations resulting therefrom. Using this additional flux contribution, they obtained good agreement with shock wave profiles, these data furnishing another class of standard non-local-equilibrium gas flow problems apart from those involving flow in microchannels. Dadzie and Reese [28], pointed out the same additional diffuse mass-density flux term to lead correct predictions of certain data in the slip-transition regime, including specifically the enhanced mass flow rate phenomenon in microchannels [29], an observation confirmed separately also by Veltzke and Thaming [30]. The present article contributes to the further development of this subject.

Our paper is organized as follows: In Sec, II we present a fully mechanically and thermodynamically consistent set of hydrodynamic equations focused on a model of volume transport that incorporates the preceding diffusive mass-volume flux contribution. Subsequently we solve this set of equations so as to obtain the velocity profile, pressure field, and mass flow rate for the case of pressure-driven flow in a rectangular microchannel. Following these calculations, Sec. III first investigates the possibility of a subatmospheric variable viscosity model, via its comparison with experimental viscosity data, to explain the phenomenon of an enhanced mass flow rate. This investigation shows variable viscosity models to be aphysical. The second investigation, one based on the volume-diffusion model, shows the success of this model towards rationalizing the data without using any fitting parameters. All theoretical predictions are compared with the recent data of Ewart *et al.* [8] using gaseous helium. Final sections of the paper present a discussion of our results together with the conclusions to be drawn therefrom.

II. AN ANALYTICAL MODEL OF A MICROCHANNEL PRESSURE-DRIVEN FLOW

A. Diffuse volume flux hydrodynamic equations

Appearing in the following equations is the material derivative, defined as $D/Dt = \partial/\partial t + U_m \cdot \nabla$. The set of hydrodynamic equations considered is written:

$$\frac{D\rho}{Dt} = -\rho \nabla \cdot U_m, \tag{1a}$$

$$\rho \frac{DU_m}{Dt} = -\nabla \cdot \mathbf{\Pi}, \tag{1b}$$

$$\rho \frac{D}{Dt}\left[\frac{1}{2}U_m^2 + e_{\text{in}}\right] = -\nabla \cdot [\mathbf{\Pi} \cdot U_v] - \nabla \cdot \mathbf{J_u}, \tag{1c}$$

closed with

$$\mathbf{\Pi} = p\mathbf{I} + \mathbf{\Pi}_v, \tag{2a}$$

$$\mathbf{\Pi}_v = -2\mu \overline{\overline{\nabla U_v}}^{\circ}, \tag{2b}$$

$$\mathbf{J_u} = -k' \nabla T, \tag{2c}$$

$$U_v = U_m + \mathbf{J}_v = U_m + \frac{\kappa_m}{\rho}\nabla \rho, \tag{2d}$$

where

$$\overline{\overline{\nabla U_v}}^{\circ} = \tfrac{1}{2}(\nabla U_v + \overline{\nabla U_v}) - \tfrac{1}{3}\nabla \cdot U_v \mathbf{I}. \tag{3}$$

The single bar over the velocity gradient denotes the transpose operator, with $\mathbf{I}$ the idemfactor. In the above set of Eqs. (1a) to (2d): ρ is the mass density, p the pressure, T the temperature, and e_{in} the fluid's mass-specific internal energy density, the latter related to the temperature by $e_{\text{in}} = (3/2)RT$, with R the specific gas constant. In terms of velocity, U_m is the mass-current velocity (or, simply, "mass velocity"), being proportional to the mass flux and satisfying the continuity equation (1a). U_v, termed the "volume velocity," is defined by expression (2d). As noted, this velocity subsequently appears in the respective constitutive equations for the shear stress entering into the momentum equation, and in the rate-or-working term entering into the energy equation. The phenomenological transport coefficients involved consist of μ the fluid-dynamic viscosity, κ_m the volume diffusivity coefficient, and $k' = kc_v/c_p$, with k the Fourier thermal conductivity, namely, the conductivity appearing in the Prandtl number, with c_v and c_p the specific heat conductivities (see Ref. [31], section 5.4.1] and Ref. [32], section 5.2]).

The set (1a) to (2d) can also be written in an alternative, conservative form as follows:

$$\frac{\partial \rho}{\partial t} + \nabla \cdot [\rho U_m] = 0, \tag{4a}$$

$$\frac{\partial}{\partial t}[\rho U_m] + \nabla \cdot [\rho U_m U_m] + \nabla \cdot [p\mathbf{I} + \mathbf{\Pi}_\mathbf{v}] = 0, \tag{4b}$$

$$\frac{\partial}{\partial t}\left[\frac{1}{2}\rho U_m^2 + \rho e_{\text{in}}\right] + \nabla \cdot \left[\left(\frac{1}{2}\rho U_m^2 + \rho e_{\text{in}}\right) U_m\right] + \nabla \cdot [(p\mathbf{I} + \mathbf{\Pi}_\mathbf{v}) \cdot U_v] + \nabla \cdot \mathbf{J}_\mathbf{u} = 0. \tag{4c}$$

The necessity for adding a diffuse volume flux to the Navier-Stokes-Fourier equations can be traced back to a work of Brenner [33]. He later proposed a slightly modified version of his first hypothesis (see Refs. [24,32,34]). The rationale for Brenner's diffuse volume flux proposal is based upon the classical principles of linear irreversible thermodynamics, a macroscopic nonkinetic model. So, in his analysis, the structure of the volume flux and the heat flux were primarily presented in order to satisfy Onsager reciprocity and symmetry principles. To obtain this agreement it has been shown that the volume diffusivity coefficient is given by $\kappa_m = k/(\rho c_p)$; that is, this diffusivity is synonymous with the fluid's thermometric diffusivity. Importing constitutive equations of all diffusive fluxes as given in Refs. [24,32,34] into the classical conservation set of equations, the resulting set of hydrodynamic equations thereby obtained is of the form written in Eqs. (4a)–(4c). Dadzie and Reese [35] proposed an alternate rationale based upon a microscopic volume-based kinetic model. Their model reduces to the set (1a)–(2d) under assumptions consisting of neglecting nonlinear diffusive fluxes, and of assuming constitutive equations for the remaining linear fluxes [36]. Following these developments, the momentum equation (1b), closed with (2b), was also derived by Koide and Kodama [27], who used a more explicit spatial stochastic approach pointing out the subtle difference from a stochastic derivative point of view. However, those authors did not provide an energy equation to accompany their mass and momentum equations. While questions arose regarding the consistency of hydrodynamic models of this type, i.e., involving different types of velocities or, equivalently, a diffusive flux driven by a mass-density gradient, a detailed analysis and explanation of these previous misinterpretations are now given in Refs. [36,37]. Thus the above set (1a)–(2d) is fully consistent with all of the known principles of mechanics. For completeness and clarity, formal confirmation of this consistency is set forth explicitly in the Appendix.

B. A volume diffusion pressure-driven flow model

Consider a steady-state, isothermal, pressure-driven flow occurring in a rectangular microchannel. The set of equations (1a)–(2d) for that configuration reduces to

$$\nabla \cdot [\rho U_m] = 0, \tag{5a}$$

$$\nabla \cdot [\rho U_m U_m] = -\nabla p - \nabla \cdot \mathbf{\Pi}_\mathbf{v}, \tag{5b}$$

$$\mathbf{\Pi}_\mathbf{v} = -2\mu \overset{\circ}{\overline{\nabla U_v}}, \tag{5c}$$

$$\mathbf{J}_v = \frac{\kappa_m}{\rho}\nabla\rho, \tag{5d}$$

$$U_v = U_m + \mathbf{J}_v. \tag{5e}$$

The height and width of the channel are denoted, respectively, by h and w, wherein $w \gg h$ such that the flow may be supposed two-dimensional, with $U_m = U_m(x,y)$ the main velocity component in the streamwise direction. The channel height-to-length ratio, h/L, was assumed to be small in the course of deriving the above set of equations. Their derivation was effected by using this small aspect ratio as a perturbation parameter in a formal regular expansion scheme, jointly with appropriate scalings of the velocity and pressure fields. Terms of dominant order in pressure and density were found to be functions only of the streamwise flow coordinate x; the cross-sectional coordinate will be denoted y. Note that this situation is compatible with Ewart's rectangular minichannel experimental setup, data from which will be used later to compare our volume-based theory with experiment [8].

1. Boundary conditions

We represent the components of the several velocity and diffuse volume flux fields as follows:

$$U_m = u_{m_x}\vec{x} + u_{m_y}\vec{y}, \tag{6}$$

$$U_v = u_{v_x}\vec{x} + u_{v_y}\vec{y},$$

$$\mathbf{J}_v = J_v\vec{x},$$

$$J_v = \kappa_m \nabla \ln\rho = \frac{k}{c_p\rho}\nabla\ln\rho. \tag{7}$$

The condition that channel walls be impermeable to mass requires that normal component of the mass velocity U_m vanish at $y = \pm h/2$. Moreover, we allow a slip form of boundary condition with respect to the volume velocity so that all boundary conditions are written:

$$u_{m_y}(x, \pm h/2) = 0 \tag{8a}$$

and

$$u_{v_x}(x,\pm h/2) = J_v(x,\pm h/2) = \mp K_{\text{slip}}\lambda_o\rho_o\frac{1}{\rho}\left[\frac{\partial u_{v_x}}{\partial y}\right]_{y=h/2} = \mp K_{\text{slip}}\lambda_o\rho_o\frac{1}{\rho}\left[\frac{\partial u_{m_x}}{\partial y}\right]_{y=h/2}, \tag{8b}$$

in which subscript o, refers to the channel outlet, which is simply used here as a convenient, albeit arbitrary, reference. Consequently, λ_o is the mean-free path at the channel outlet. We note that Eq. (8b) is not a standard slip condition, as the equation can be viewed as a constitutive equation for the volume flux $\mathbf{J}_v$ at the boundary when $u_{m_x} = 0$ (i.e., when there is no slip imposed on the mass velocity). As such, slip coefficient K_{slip} is simply incorporated into that expression for the purpose of effecting comparisons with theoretical expressions obtained by conventional slip models. Otherwise, it will be seen later, when the volume diffusion description is adopted, that this slip coefficient is not necessarily required to obtain agreement with experiments.

2. A solution method

The continuity and momentum equations (5a) and (5b) may be respectively rewritten for this pressure-driven

flow as

$$\rho\frac{\partial u_{m_x}}{\partial y}+\frac{\partial}{\partial x}[\rho u_{v_x}]-\frac{k}{c_p}\frac{d^2\ln\rho}{dx^2}=0, \tag{9a}$$

$$\mu\frac{\partial^2 u_{v_x}}{\partial y^2}=\frac{dp}{dx}. \tag{9b}$$

The solution of Eq. (9b) satisfying boundary condition (8b) is

$$u_{v_x}=\frac{1}{8\mu}\frac{dp}{dx}\left(4y^2-h^2-8\frac{\mu}{\rho}E\right), \tag{10}$$

in which

$$E=K_{\rm slip}\frac{h^2{\rm Kn}_o}{2\nu_o}, \tag{11}$$

wherein ν_o denotes the kinematic viscosity at the outlet, and

$${\rm Kn}_o=\frac{\lambda_o}{h} \tag{12}$$

is the outlet Knudsen number. Substitute (10) into (9a) and solve the resulting expression for u_{m_x} subject to boundary condition (8a), so as to obtain

$$u_{m_x}=-\frac{1}{8\mu}\left(\frac{4}{3}y^3-h^2y\right)\frac{1}{\rho}\frac{d}{dx}\left[\frac{\rho dp}{dx}\right]+Ey\frac{1}{\rho}\frac{d^2p}{dx^2}+y\frac{k}{c_p\rho}\frac{d^2\ln\rho}{dx^2}+C(x), \tag{13}$$

where the integration constant $C(x)$ is a function only of x. However, application of boundary conditions (8b) requires that $C(x)=0$ as a result of symmetry. The preceding equations furnish the pressure distribution in accordance with the following scheme. Evaluate equation (13) at $y=\pm h/2$, and use boundary condition (8b) to obtain

$$\frac{1}{12}h^2\frac{d}{dx}\left[\frac{\rho dp}{dx}\right]+E\frac{d^2p}{dx^2}+\frac{k}{c_p}\frac{d^2\ln\rho}{dx^2}=0. \tag{14}$$

Eliminate the density in equation (14) in favor of the pressure via use of the ideal gas law $p=\rho RT$, and subsequently use the identity $pdp/dx=(d/dx)(p^2/2)$ to obtain

$$\frac{d}{dx^2}\left[p^2+\frac{24\mu RT}{h^2}\left(Ep+\frac{k}{c_p}\ln p\right)\right]=0. \tag{15}$$

Integration of Eq. (15) followed by rearrangement yields

$$\left(\frac{p}{p_o}\right)^2+F\frac{p}{p_o}+G\left[\ln\left(\frac{p}{p_o}\right)+\ln p_o\right]=C\frac{x}{L}+D, \tag{16}$$

where

$$F=\frac{24\mu RT}{h^2p_o}E\quad\text{and}\quad G=\frac{24\mu RT}{h^2p_o^2}\frac{k}{c_p}.$$

Alternatively, in terms of the Knudsen and Prandtl numbers,

$$F=12K_{\rm slip}{\rm Kn}_o\quad\text{and}\quad G=\frac{24}{{\rm Pr}k_\lambda^2}{\rm Kn}_o^2,$$

where k_λ is a coefficient associated with the definition of the mean-free path as related to the choice of molecular collision model. It is often quoted as having the value $k_\lambda=\sqrt{\pi/2}$ (see Ref. [38]).

Equation (16) is the pressure distribution, in which the constants C and D are determined from knowledge of the channel inlet and outlet pressures, $p(x=0)=p_i$ and $p(x=L)=p_o$. This furnishes the expression

$$\begin{aligned}C&=-[(P^2-1)+F(P-1)+G\ln P]\quad\text{and}\\ D&=P^2+FP+G(\ln P+\ln p_o),\end{aligned} \tag{17}$$

where

$$P=\frac{p_i}{p_o} \tag{18}$$

denotes the inlet-to-outlet pressure ratio. Substitution into (16) of the constants from Eq. (17) yields

$$\left(\frac{p}{p_o}\right)^2+F\frac{p}{p_o}+G\ln\left(\frac{p}{p_o}\right)=(P^2+FP+G\ln P)\left(1-\frac{x}{L}\right)+(1+F)\frac{x}{L}. \tag{19}$$

3. *Mass flow rate*

The mass flow rate through the channel is given by the expression

$$\dot M=w\int_{-h/2}^{h/2}\rho U_m dy=\text{const}. \tag{20}$$

Rearrangement of Eq. (5e) gives $U_m=U_v-\mathbf{J}_v$. Hence, with use of Eqs. (10) and (7) we have that

$$u_{m_x}=\frac{1}{8\mu}\frac{dp}{dx}\left(4y^2-h^2-8\mu E\frac{1}{\rho}\right)-\frac{k}{c_p\rho}\frac{d\ln\rho}{dx}. \tag{21}$$

Multiply Eq. (21) by ρ and subsequently eliminate ρ in favor of p on the right-hand side. Introduction of the resulting expression into Eq. (20) yields

$$\dot M=-\frac{wh^3}{24\mu RT}\frac{d}{dx}\left[p^2+\frac{24\mu RT}{h^2}\left(Ep+\frac{k}{c_p}\ln p\right)\right]. \tag{22}$$

The bracketed term in Eq. (22) is seen to be identical to the bracketed term in Eq. (15). It follows that

$$\dot M=-\frac{wh^3p_o^2}{24L\mu RT}C, \tag{23}$$

where C is the constant given by Eq. (17). Thus, the mass flow rate is given as

$$\dot M=\frac{wh^3p_0^2}{24L\mu RT}\left[(P^2-1)+12K_{\rm slip}{\rm Kn}_o(P-1)+\frac{24}{{\rm Pr}k_\lambda^2}{\rm Kn}_o^2\ln P\right]. \tag{24}$$

For subsequent use in our appraisal of the significance of the latter result it is convenient to rewrite it in the following generic form:

$$\dot M=\frac{wh^3p_0^2}{24L\mu RT}(P^2-1)\left[1+A{\rm Kn}_o\frac{1}{P+1}+B{\rm Kn}_o^2\frac{\ln P}{P^2-1}\right], \tag{25}$$

in which the various coefficients appearing therein are summarized in Table I.

TABLE I. Summary of the coefficients appearing in the mass flow rate equation (25).

A	B	P	Pr	Kn_o	k_λ	Sc	K_{slip}	λ
$12K_{\mathrm{slip}}$	$\frac{24}{\mathrm{Pr}k_\lambda^2}$	p_i/p_o	$c_p\mu/k$	λ_o/h	$\frac{\sqrt{\pi}}{2}$	$\mu/(\rho\kappa_m)$	$\frac{\sqrt{\pi}}{2}\times\frac{\sqrt{2}}{k_\lambda}$	$k_\lambda\frac{\mu}{p}\sqrt{2RT}$

Depending upon the choice of coefficients appearing therein, Eq. (25) for the mass flow rate possesses the general structure expected of any nonkinetic model of pressure-driven flow in a microchannel. For example, upon setting $A = B = 0$ therein one obtains the Navier-Stokes compressible gas flow result for the case where there is no slip of the mass velocity, namely,

$$\dot{M} = \frac{wh^3 p_0^2}{24L\mu RT}(P^2 - 1). \tag{26}$$

Similarly, setting $B = 0$ furnishes the mass flow rate for the case where first-order slip boundary conditions prevail:

$$\dot{M} = \frac{wh^3 p_0^2}{24L\mu RT}(P^2 - 1)\left[1 + A\mathrm{Kn}_o\frac{1}{P+1}\right]. \tag{27}$$

Last, with $A = 0$ we obtain

$$\dot{M} = \frac{wh^3 p_0^2}{24L\mu RT}(P^2 - 1)\left[1 + B\mathrm{Kn}_o^2\frac{\ln P}{P^2-1}\right]. \tag{28}$$

Equation (28) is obtained when the volume diffusion hydrodynamic model equations are solved subject to a no-slip boundary condition imposed on the volume velocity at the channel walls, i.e., $u_{v_x}(x,\pm h/2) = 0$ in Eq. (8b). In that particular case it follows from the relation between the mass and volume velocities in Eq. (5e) that the second term in Eq. (28) is a form of slip generated by the presence of the new diffuse volume flux contribution. As such, it does not strictly constitute a boundary effect. Retention of both A and B in the mass flow rate expression (25) may be viewed as a slip velocity model wherein the second term, due to B, is associated with second-order boundary effects, following the first-order slip contribution arising from A. However, corrections arising from inclusion of this latter term will subsequently be seen as not particularly impressive with respect to agreement with experimental data [15], in addition to being subject to questioning on physical grounds [13]. Graur *et al.* [38], using their "quasi-gas dynamics equation," derived an equation of exactly the form of Eq. (25). When comparing their theoretical results with experiments they adopted for the B coefficient the value $24/k_\lambda^2$, which in fact is associated with a Schmidt or Prandtl number value of unity. Their agreement with experiments covers only the slip regime. Dongari *et al.* [16] obtained an expression of the form (28) when modeling the mass flux appearing in the continuity equation as consisting of a superposition of convective and diffusive portions. The latter authors, upon combining their scheme with a variable mean-free path model, while also adopting a Prandtl number value of unity, obtained moderate agreement with experiment over the full Knudsen number regime. However, the value of the mass flow rate at the Knudsen minimum was underpredicted in comparison with experimental data, with deviations observed in the transition regime. In contrast with their Prandtl number choice of unity, our comparison with data, effected later in Sec. III is performed using an exact Prandtl number value of 2/3 for the helium data.

In the course of gas-kinetic description of the hydrodynamic model of Eqs. (1a)–(2d), volume diffusion is understood to arise from a molecular-level spatial diffusion process [35]. This, in turn, generates a second level of scaling beyond, or parallel to, traditional Knudsen number scaling [37]. Therefore, we assume following the recent work by Veltzke and Thaming [30], that the volume diffusivity coefficient depends not only on the properties of the gas but also on the geometry of the channel. This leads us to identify a geometry-dependent volume diffusivity coefficient for the rectangular channel as

$$\kappa_m^* = \kappa_m\frac{L}{w} = \frac{kL}{\rho c_p w}, \tag{29}$$

thus ascribing to the B coefficient the following geometry-dependent formula for the case of rectangular channels:

$$B = \frac{24}{\mathrm{Sc}k_\lambda^2}\frac{w}{L} \quad \text{or} \quad B = \frac{24}{\mathrm{Pr}k_\lambda^2}\frac{w}{L}, \tag{30}$$

in which Schmidt and Prandtl numbers retain their standard values. Imposing $K_{\mathrm{slip}} = 1$ is tantamount to interpreting boundary condition (8b) as a simple constitutive equation for the volume flux $\mathbf{J}_v$. Introduction of Eq. (30) into Eq. (24) furnishes a formula for the mass flow rate, one given by the volume diffusion hydrodynamic model as

$$\dot{M} = \frac{wh^3 p_0^2}{24L\mu RT}\left[(P^2-1) + 12\mathrm{Kn}_o(P-1) + \frac{24w}{\mathrm{Pr}Lk_\lambda^2}\mathrm{Kn}_o^2\ln P\right], \tag{31}$$

in which, there appear only physical properties with none of the coefficients playing a role of a fitting parameter. This final expression will subsequently be used in the context where Eq. (25) is associated with our volume diffusion model.

III. COMPARISON WITH EXPERIMENTS

A. A variable viscosity coefficient in fitting the experiments

At early stages of the observation of unconventional behavior during low-pressure gas flows, some authors questioned the dependence of the transport coefficients on pressure, suspecting this as a possible explanation of phenomena such as the Knudsen enhanced mass flow rate [39]. The average pressure in the experiments conducted by Ewart *et al.* [8], whose data are adopted here as the experimental benchmark in our paper, ranges from 67 000 to 30 Pa. As such, the typical subatmospheric pressure range encountered in their experiments involved the very low pressure region. To explore this issue, our analysis begins by scrutinizing the effect of pressure-induced variations in viscosity on the mass flow rate, while viewing this effect purely in the context of its impact

on the slip velocity occurring at the microchannel walls, i.e., solely on the grounds of its role in affecting momentum diffusion.

Kinetic theory assumes transport coefficients to be solely a function of temperature, independent of pressure [10] (due to prioritizing molecular collisions as the only source of diffusion). An experimental viscosity-temperature power law for helium given by Peterson [40] reads

$$\mu = \frac{1.865 \times 10^{-5}}{T_{ao}^{0.7}} T^{\alpha} = 3.676 \times 10^{-7} \times T^{\alpha}, \qquad (32)$$

where T_{ao} is the absolute $0\,^{\circ}\mathrm{C} = 273$ K temperature and α is the viscosity exponent. This exponent is frequently manipulated as a fixed value. For helium, for example, its value given by Bird [41] is 0.66. However, Greenshields and Reese [42], in their investigations of shock wave structures, found that this viscosity exponent can vary according to flow regimes. They provided values of this exponent over different ranges of Mach number, varying from 0.68 to 0.76, and respectively encompassing Mach numbers lower than 4 to 12.5.

Adopting viscosity-temperature power law formula (32), and assuming the viscosity exponent a function of a pressure, our analysis of the data of Ewart *et al*. shows that equation

$$\alpha = a_{\alpha} \ln p_m + b_{\alpha} \qquad (33)$$

for this viscosity exponent can reproduce Ewart's experimental mass flow rate data, where $p_m = (p_i + p_o)/2$ represents the average pressure in the channel, using mass flow rate equation (28). With this mass flow equation and viscosity given by Eq. (33), we extract from Ewart's experimental data the values $a_{\alpha} = 0.0586$ and $b_{\alpha} = 0.0204$. Figure 1 compares the respective mass flow rate equations (26) and (28) with the experimental data obtained by this scheme. Essentially we observe in the vanishingly small Knudsen number regime that use of variable viscosity formula (33) (evaluated at the mean pressure p_m) in the denominator of the constant viscosity Navier-Stokes formula (26) shows some improvements over the comparable constant viscosity case. Meanwhile, Eq. (28)

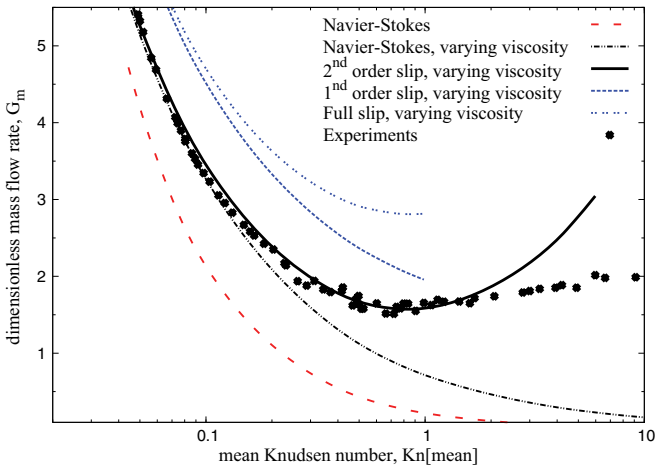

FIG. 1. (Color online) Comparison of theoretical mass flow rate predictions using the variable viscosity model with experiments. Note that "second-order slip varying viscosity" as given by Eq. (28) gives the best fit in this case.

TABLE II. Summary of fluid properties and physical coefficients used in Fig. 3.

w	L	h	Pr
4.92×10^{-4} [m]	9.39×10^{-3} [m]	9.38×10^{-6} [m]	0.67
μ	k_{λ}	Sc	P
1.97513×10^{-5} [Pa s]	$\sqrt{\pi/2}$	0.67	5

covers the data to above Kn = 1. This value is obtained using a Prandtl number for helium of Pr = 0.67, the geometrical characteristic of Ewart's experimental microchannel as reported in Table II. All our flow rate graphs are plotted in the form of a dimensionless flow rate G_m versus the mean Knudsen number defined as

$$\mathrm{Kn[mean]} = k_{\lambda} \frac{\mu}{\frac{p_i + p_0}{2}} \sqrt{2RT}. \qquad (34)$$

In general, Fig. 1 shows that whereas allowing the viscosity coefficient to be a variable, rather than a constant results in some improvement in the accuracy of the Navier-Stokes model, this improvement deteriorates if, at the same time, the first-order slip term is integrated in conjunction with this varying viscosity. Our next comparison demonstrates the inappropriateness of varying viscosity models.

In order to assess validity of viscosity coefficient obtained in Eq. (33) we compare the predicted and experimental viscosities in what follows. Experimental values at pressures above atmospheric are abundant, all such data confirming that the viscosity is indeed insensitive to pressure in that case. However, viscosity data in the range 30–67 000 Pa (and at an ambient temperature) are far less abundant. Itterbeek and Paemel [43] provide measurements at low pressures and low temperature, pointing out the effects of pressure dependence, while proposing a phenomenological correlation thereof. Data provided by Shimotake and Thodos [44] offered the best compromise in the low-pressure range. Although their measurements fall into a low-temperature region, their data show a clear uniform profile that can be extrapolated to ambient temperatures. We report these viscosity data in Fig. 2. Exact measurements correspond to temperatures of 15, 30, and 127 K. Also provided is an extrapolated graph for 297 K, the latter displaying consistency with the other profiles. Collectively, these data furnish a well-defined correlation governing the functional dependence of viscosity upon pressure. The viscosity coefficient points to a dramatic decrease with pressure from about 30 Pa and below. For pressures above that threshold value the viscosity asymptotes to a constant value that depends upon the temperature.

In Fig. 2 we also plot viscosity data from Ewart's experiments, that is to say, with the exponent given by Eq. (33). It appears that viscosity values fitting the experimental mass flow rate data are in complete disagreement with their experimental viscosity counterparts. There is no comparison with the experimental viscosity-pressure dependence. In contrast, coincidentally, the region where the viscosity data starts to decrease dramatically with pressure appears to be the end of the range of Ewart's experimental data. We conclude that viscosity is nearly constant, on average, over the main portion of the mass flow rate experiments.

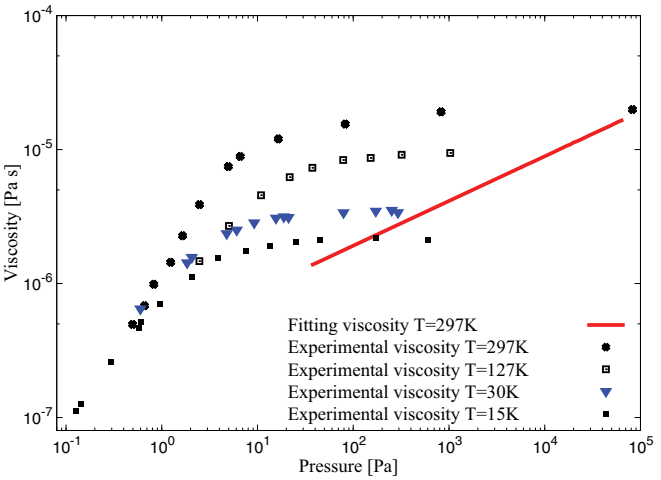

FIG. 2. (Color online) Comparison between viscosity values fitting Ewart *et al.*'s [8] experimental data and the true experimental viscosity data: "Fitting viscosity values" are those viscosities obtained using Eq. (32) with Eq. (33), whereas "experimental viscosity" data are those given by Ref. [44].

In effecting the above comparison the first- and second-order terms in Eq. (25) were based on traditional slip velocity concepts. We note that the notion of a variable viscosity exponent, as in Eq. (33), is highly compatible with the kinetic-theory description of viscosity as a physical concept. This is so because viscosity is obtained from the Boltzmann collision integral using a chosen molecular interaction potential [10]. In other words, varying the viscosity exponent is tantamount to varying the interaction potential. We therefore interpret the mismatch between experimental viscosity and viscosity fitting the mass flow data, as an inability of a variable viscosity model, and to some extent a single momentum diffusion model, to explain the enhanced mass flow rate phenomenon.

B. The role of volume diffusivity in determining the mass flow rate: Knudsen diffusion in microchannels

In this section the viscosity coefficient spanning the temperature and pressure range of the Ewart *et al.* [8] experiments is taken to be a constant with respect to the observations in Fig. 2. This value is reported in Table II. Furthermore, the coefficient K_{slip} is set equal to unity, such that boundary condition (8b), which concerns the volume flux rather than the mass velocity, now appears as a constitutive equation governing the volume flux at the boundary. The mass flow rate in this case is therefore given exclusively by our Eq. (31), which contains a volume diffusivity coefficient, namely, that given by Eq. (29).

Dimensional, rather than nondimensional, mass flow rates are presented in order to allow direct comparison with the exact experimental values given in the table in the appendix of Ref. [8]. Subsequently, both experimental and theoretical expressions are rendered in the same dimensionless form using the following equation:

$$G_m = \dot{M}\left[\frac{wh^2}{L\sqrt{2RT}}(p_{\text{in}} - p_{\text{out}})\right]^{-1}. \qquad (35)$$

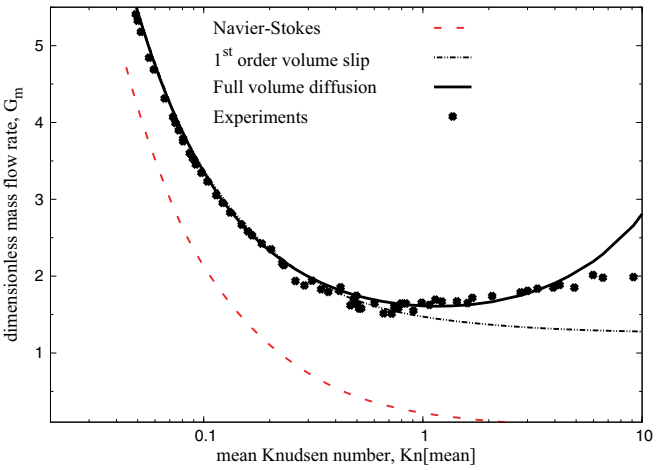

FIG. 3. (Color online) Volume diffusion hydrodynamic predictions of mass flow rate compared with experiments.

Values of the fluid properties and channel dimensions required in order to calculate theoretical values from Eq. (31) are summarized in Table II. In this table no adjustable or fitting coefficient is involved.

Figure 3 shows predictions based upon the volume diffusion hydrodynamic models. Observe that the Navier-Stokes model modified by use of the first-order volume diffusion boundary condition furnishes good agreement up to a Knudsen number of unity. The full volume diffusion hydrodynamic model, i.e., Eq. (31) agrees with the data up to a Knudsen number of about 5, with all parameters possessing clear physical meanings as given in Table II and a viscosity coefficient having its appropriate experimental value.

For further analysis we compare the relative contributions of slip and volume diffusion to the total mass flow rate in Fig. 4. Slip constitutes the source of the first-order term in Eq. (25).

The contribution due to slip appears constant throughout all Knudsen number regimes, while the diffusion of volume appears to have an ever-greater contribution as the Knudsen number increases.

A contradiction exists between experimental observations in Fig. 4 and the interpretation assigned to the first-order

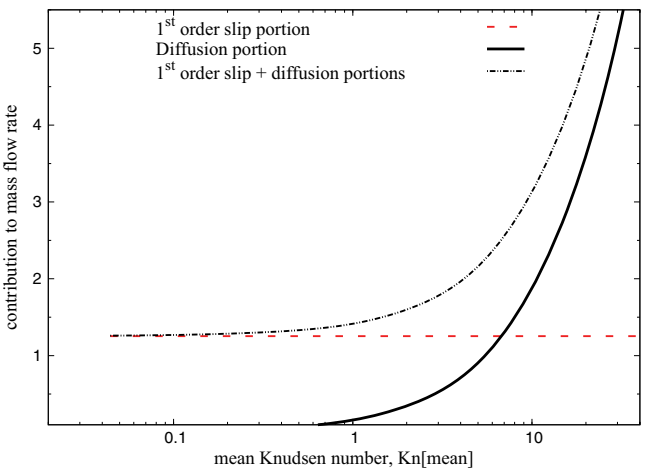

FIG. 4. (Color online) Comparison of slip and volume diffusion contribution to the mass flow rate.

correction to the mass rate of flow as arising from traditional velocity slip. Indeed, the latter is regarded as the source of surface-effect corrections that are only valid in the slip regime, namely, in the approximate range of Knudsen numbers $0.01 < \mathrm{Kn} < 0.1$ [1]. Accordingly, having a constant amount of slip for all Knudsen numbers, up to and including the free-molecule regime, is rather a contradiction.

In fact, fluctuations in local number of molecules are expected to become more sensitive as rarefaction effects increase or the gas becomes confined in a small geometry. A volume diffusion is indeed a molecular spatial diffusion effect. As such, matching between the experimental data and this diffusion model is rather compatible. The rapid decrease of viscosity with pressure revealed by experimental data (see Fig. 2) as the pressure tends to zero may be invoked to explain the divergence of the volume diffusion model from the experimental mass flow rate data in that portion of the graph extending into the free-molecule regime. Overall, the phenomenon of volume diffusion appears to provide a sound interpretation of the data.

IV. DISCUSSION: COMPARISON WITH A STOCHASTIC KINETIC-MOLECULAR MODEL

In Refs. [20,21], the following stochastic model of molecular motion was solved in an attempt to explain experimentally observed phenomena pertaining to the enhanced mass flow rate and to the Knudsen minimum:

$$\begin{aligned} \frac{\delta X_i}{\delta t} &= M_i, \\ \frac{\delta M_i}{\delta t} &= -\frac{1}{\tau}(M_i - U_i) + \left(\frac{4e_{\mathrm{in}}}{3\tau}\right)^{1/2} \frac{\delta Wi(t)}{\delta t}, \end{aligned} \tag{36}$$

where X_i refers to molecular position and M_i to molecular velocity. τ is a relaxation parameter, and $Wi(t)$ denotes a Wiener process, representing a stochastic force component. Good agreement was reported by the authors with the argon data of Dong [22] up to Knudsen numbers of five, with excellent detail being displayed in the transition regime. This represents the same good agreement as was observed in the case of Ewart's helium data for the present volume diffusion hydrodynamic model. While Jenny *et al.* [21] originally described their model as an alternative to modeling the Boltzmann collision integral, Eqs. (36) also qualify in our view as a kinetic form of the volume-mass diffusion hydrodynamic model [25].

Indeed, in Eqs. (36) we note that the molecular position variable X_i and molecular velocity (momentum) variable M_i are not independent; rather, they are coupled. Furthermore, the position variable X_i (as well as the time variable) in Eqs. (36) is not the position variable that appears in continuum-type equations. This distinction was clearly recognized in Ref. [20, p. 8], where these variables were distinguished notationally, with one designated as x and the other as X. In addition, in stochastic equations such as that in Eqs. (36) involving especially a Wiener operator, derivative operators no longer mean a derivative in the ordinary sense but need to be treated in the Itô sense. That is to say, we need both a definition of a measure and the use of the Itô integration formula in order to perform any analytical integration or comparison. This explicit integration has been performed by Bogomolov and Dorodnitsyn [23], who derived a macroscopic set of equations associated with Eqs. (36). Taking into account the fact that displacement is given by the time integral of the velocity and the Itô transformation, with a certain Knudsen number consideration, Bogomolov and Dorodnitsyn derived a corresponding set of hydrodynamic equations in which density obeys the equation:

$$\frac{\partial \rho}{\partial t} + \nabla \cdot [\rho U - \mathrm{Kn}_{\mathrm{loc}} \kappa_m \nabla \rho] = 0, \tag{37}$$

which is a diffusive volume type of equation for the density (wherein κ_m corresponds to $\sim 0.5 D^2/A^2$ of Ref. [20]). Note that the diffusive term in Eq. (37) derives directly from the second term in the Itô formula. Physically, it represents the translation of the stochasticity implemented on the velocity in Eqs. (36) onto particle positions. $\mathrm{Kn}_{\mathrm{loc}}$ is a local Knudsen number-like parameter, which is the signature of the transition from the molecular position variable X_i to the continuum position variable x.

In our Eq. (4a), substitution of the mass velocity U_m for the volume velocity U_v together with use of the modified volume diffusivity coefficient in Eq. (29) yields Eq. (37) exactly. Although it is an equation possessing a diffuse volume component, it does not constitute a true physical dissipation or mass disappearance attribute, since the diffusive contribution is not measured relative to the mass velocity. The presence of the diffuse component, either in the form as it appears in Eq. (37) or, alternatively, in the role of an additional contribution to the shear stress as embodied in Eqs. (5d) and (5e), is the principal driver in obtaining the mass flow rate (25). Volume diffusion evidently constitutes the key player in obtaining all of these agreements.

The Knudsen paradox is represented by the extremum observed in Fig. 3. In fact, a change in the behavior (change in curvature) of the mass flow rate versus Knudsen number for this pressure-driven flow, which is isothermal, may be interpreted as heralding the appearance of another transport process overtaking that of momentum diffusion. This additional point of view would appear to confirm the volume or mass diffusion interpretation of the experimental data [25,30].

V. CONCLUSIONS

In this paper we present, using nonstandard kinetic modeling, an in-depth analysis of the Knudsen-enhanced mass flow rate phenomenon in micro-gas channels. We report that while it is possible to use a pressure-dependent viscosity expression to fit the data, this technique, and to some extent a single momentum diffusion theory, does not furnish a correct interpretation of the data; rather, contradictions appear when attempting to do so. Our enhanced mass flow analysis also provides a test of the recent volume-diffusion hydrodynamic model. This model is found to accord well with existing experimental data, and in a more physically sound manner than competitive models, without necessitating the use of any fitting parameters.

APPENDIX: MECHANICAL AND THERMODYNAMIC CONSISTENCIES OF THE VOLUME-DIFFUSION HYDRODYNAMIC MODEL

The mechanical and thermodynamic requirements that need to be satisfied by any hydrodynamic model are described and listed in Ref. [45]. They are:

(i) Galilean invariance
(ii) Integrability
(iii) Angular momentum conservation
(iv) Steady rigid-body fluid rotation
(v) Center-of-mass position
(vi) Second law of thermodynamics.

Consider the proposed set of hydrodynamic equations (1a)–(2d) in which the material derivative is formulated, as usual, with respect to U_m. For clarity, the conservative forms of these hydrodynamic equations are repeated here:

$$\frac{\partial \rho}{\partial t} + \nabla[\rho U_m] = 0, \tag{A1a}$$

$$\frac{\partial}{\partial t}[\rho U_m] + \nabla \cdot [\rho U_m U_m] = -\nabla \cdot [p\mathbf{I} + \mathbf{\Pi}_\mathbf{v}], \tag{A1b}$$

$$\frac{\partial}{\partial t}\left[\frac{1}{2}\rho U_m^2 + \rho e_{\text{in}}\right] + \nabla \cdot \left[\left(\frac{1}{2}\rho U_m^2 + \rho e_{\text{in}}\right) U_m\right] = -\nabla \cdot [(p\mathbf{I} + \mathbf{\Pi}_\mathbf{v}) \cdot U_v] - \nabla \cdot \mathbf{J}_\mathbf{u}. \tag{A1c}$$

According to Eq. (A1a) the mass flux is given by ρU_m, with this flux being synonymous with the momentum density appearing in the momentum transport [Eq. (A1b)].

1. Galilean invariance

Consider the following transformation:

$$\begin{aligned} \hat{t} &= t, \\ \hat{X} - ct &= X, \\ \hat{U}_m - c &= U_m, \end{aligned} \tag{A2}$$

where the vector c denotes some constant velocity. Equations (A2) furnish the following transformed partial time and position derivatives:

$$\begin{aligned} \frac{\partial}{\partial t} &= \frac{\partial}{\partial \hat{t}} + c \cdot \frac{\partial}{\partial \hat{X}}, \\ \frac{\partial}{\partial X} &= \frac{\partial}{\partial \hat{X}}. \end{aligned} \tag{A3}$$

These, in turn, yield the transformed material derivative:

$$\frac{D}{Dt} = \frac{\partial}{\partial t} + U_m \cdot \nabla = \frac{\partial}{\partial \hat{t}} + \hat{U}_m \cdot \nabla = \frac{D}{D\hat{t}}, \tag{A4}$$

thus rendering the material derivative galilean invariant. Substitution of this material derivative together with the change of variable (A2) into the mass and momentum equations (1a) and (1b), subsequently followed by closure of the scheme by use of Eq. (2b), is seen to furnish the same forms of equations as above. Moreover, the expressions for the diffuse volume flux, heat flux, and shear stress as given in Eqs. (2a)–(2d) are all Galilean invariant.

The energy equation (A1c) can be rewritten by using the momentum and mass equations as follows:

$$\begin{aligned} \rho \frac{De_{\text{in}}}{Dt} = &-p\mathbf{I} : \nabla U_m - \mathbf{\Pi}_{Um} : \nabla U_m - \mathbf{\Pi}_\mathbf{Jv} : \nabla U_m \\ &- \nabla \cdot [p\mathbf{I} \cdot \mathbf{J}_v] - \nabla \cdot [\mathbf{\Pi}_{Um} \cdot \mathbf{J}_v] \\ &- \nabla \cdot [\mathbf{\Pi}_\mathbf{Jv} \cdot \mathbf{J}_v] - \nabla \cdot \mathbf{J}_\mathbf{u}. \end{aligned} \tag{A5}$$

Accordingly, the energy equation is also Galilean invariant.

2. Integrability

Integrability is concerned with the transport equation for the total mass flux. In the hydrodynamic model described by Eqs. (A1a)–(A1c) the total mass flux is ρU_m. It follows that the transport equation for the total mass is just the momentum transport equation (A1b), and so is itself a conservation equation.

3. Angular momentum

Conservation of angular momentum is an important requirement of proposed hydrodynamic equations. Forming the cross-product of Eq. (1b) with hydrodynamic position vector X gives

$$X \wedge \rho \frac{DU_m}{Dt} = -X \wedge \nabla \cdot [p\mathbf{I} + \mathbf{\Pi}_\mathbf{v}]. \tag{A6}$$

This is equivalent to

$$\rho \frac{D}{Dt}[X \wedge U_m] = -X \wedge \nabla \cdot [p\mathbf{I} + \mathbf{\Pi}_\mathbf{v}]. \tag{A7}$$

Now, for a symmetrical second-order tensor $\bar{\bar{\mathrm{T}}}$, the following property holds:

$$X \wedge [\nabla \cdot \bar{\bar{\mathrm{T}}}] = \nabla \cdot [X \wedge \bar{\bar{\mathrm{T}}}]. \tag{A8}$$

The pressure tensor $\mathbf{\Pi}_\mathbf{v}$ as given in Eq. (2b) is symmetrical. As such, Eq. (A7) adopts the following final form:

$$\rho \frac{D}{Dt}[X \wedge U_m] = -\nabla \cdot [X \wedge (p\mathbf{I} + \mathbf{\Pi}_\mathbf{v})]. \tag{A9}$$

The principle of conservation of angular momentum is therefore seen to be satisfied.

4. Center-of-mass position

In the absence of external forces the center-of-mass motion must be uniform. To this end one expects the quantity

$$B = \rho X - \rho U_m t \tag{A10}$$

to be a conserved quantity. As such, we write that

$$\frac{\partial B}{\partial t} = \frac{\partial}{\partial t}[\rho X - \rho U_m t] = X\frac{\partial \rho}{\partial t} - t\frac{\partial}{\partial t}[\rho U_m] - \rho U_m, \tag{A11}$$

into which the mass and momentum equations (A1a) and (A1b) can be introduced so as to obtain

$$\frac{\partial B}{\partial t} = -X\nabla \cdot [\rho U_m] + t\nabla \cdot [\rho U_m U_m + (p\mathbf{I} + \mathbf{\Pi}_\mathbf{v})] - \rho U_m. \tag{A12}$$

Equation (A12) can be written as

$$\frac{\partial B}{\partial t} = -\nabla\cdot[\rho X U_m] + \rho U_m + t\nabla\cdot[\rho U_m U_m + (p\mathbf{I} + \mathbf{\Pi}_v)] - \rho U_m, \quad \text{(A13)}$$

or, more simply,

$$\frac{\partial B}{\partial t} = -\nabla\cdot[BU_m - t(p\mathbf{I} + \mathbf{\Pi}_v)]. \quad \text{(A14)}$$

The latter is therefore a conservative transport equation for the quantity defined by Eq. (A10). Consequently the center-of-mass position principle is satisfied.

The fundamental reason underlying satisfaction of the above set of mechanical principles (galilean invariance, integrability, angular momentum, center-of-mass position) resides in the fact that the mass flux velocity U_m is the same as the momentum density velocity. Consequently these attributes are being satisfied with respect to the mass velocity rather than with respect to the volume velocity.

5. Second law of thermodynamics

Regarding satisfaction of the second law of thermodynamics, Brenner [24] showed that the model (1a)–(2d) possesses classical irreversible thermodynamic structure in circumstances for which $\kappa_m = k/(\rho c_p)$. More generally, however, a complete form of the volume diffusion set of equations (and particularly the energy equation) is required to achieve a full structure of the second law. This is constructed, for example, in Ref. [36] without restriction to satisfaction of a modified Gibbs equation.

[1] S. Colin, *Microfluidics, ISTE* (John Wiley & Sons, New York, 2010).
[2] G. Kandlikar, S. Garimella, D. Li, S. Colin, and M. R. King, *Heat Transfer and Fluid Flow in Minichannels and Microchannels* (Elsevier, Amsterdam, 2006).
[3] G. Karniadakis, A. Beskok, and N. R. Aluru, *Microflows and Manoflows: Fundamentals and Simulations* (Springer, New York, 2005).
[4] M. Knudsen, Ann. Phys. **28**, 75 (1909).
[5] B. T. Porodonov, P. E. Suetin, S. F. Borisov, and V. D. Akinshin, J. Fluid Mech. **64**, 417 (1974).
[6] E. B. Arkilic, K. S. Breuer, and M. A. Schmidt, J. Fluid Mech. **437**, 29 (2001).
[7] J. Maurer, P. Tabeling, P. Joseph, and H. Willaime, Phys. Fluids **15**, 2613 (2003).
[8] T. Ewart, P. Perrier, I. Graur, and J. M. Meolans, J. Fluid Mech. **584**, 337 (2007).
[9] C. Cercignani, *Theory and Application of the Boltzmann Equation* (Scottish Academic Press, Edinburgh, 1975).
[10] S. Chapman and T. G. Cowling, *The Mathematical Theory of Non-Uniform Gases*, 3rd ed. (Cambridge Mathematical Library, Cambridge, 1970).
[11] F. Sharipov, J. Vac. Sci. Technol. A **17**, 3062 (1999).
[12] J. C. Maxwell, Phil. Trans. R. Soc. London **170**, 231 (1878).
[13] S. Colin, Microfluid Nanofluid **1**, 268 (2005).
[14] N. G. Hadjiconstantinou, Phys. Fluids **15**, 2352 (2003).
[15] E. J. Arlemark, S. K. Dadzie, and J. M. Reese, J. Heat Transfer **132**, 041006 (2010).
[16] N. Dongari, F. Durst, and S. Chakraborty, Microfluid Nanofluid **9**, 831 (2010).
[17] M. A. Gallis and J. R. Torczynski, Phys. Fluids **24**, 012005 (2012).
[18] J. Zhang, J. Fan, and F. Fei, Phys. Fluids **22**, 122005 (2010).
[19] K. Michalis, V. N. Kalarakis, A. D. Skouras, and E. N. Burganos, Microfluidics Nanofluidics **9**, 847 (2010).
[20] M. H. Gorji, M. Torrilhon, and P. Jenny, J. Fluid Mech. **680**, 574 (2011).
[21] P. Jenny, M. Torrilhon, and S. Heinz, J. Comput. Phys. **229**, 1077 (2010).
[22] W. Dong, Technical report, University of California, report UCRL-3353, 1956 (unpublished).
[23] S. V. Bogomolov and L. W. Dorodnitsyn, Math. Models Comp. Simulat. **3**, 457 (2011).
[24] H. Brenner, Int. J. Eng. Sci. **54**, 67 (2012).
[25] S. K. Dadzie, J. Comput. Phys. **231**, 7011 (2012).
[26] S. K. Dadzie and J. M. Reese, Phys. Lett. A **376**, 967 (2012).
[27] T. Koide and T. Kodama, arXiv:1105.6256.
[28] S. K. Dadzie and J. M. Reese, Phys. Fluids **22**, 016103 (2010).
[29] N. Dongari, S. K. Dadzie, and J. M. Reese, in *27th International Symposium on Rarified Gas Dynamics*, Vol. 1333 (AIP, New York, 2011), p. 718.
[30] T. Veltzke and J. Thaming, J. Fluid Mech. **698**, 406 (2012).
[31] H. Brenner, Physica A **349**, 11 (2005).
[32] H. Brenner, Int. J. Eng. Sci. **47**, 930 (2009).
[33] H. Brenner, Physica A **349**, 60 (2005).
[34] H. Brenner, Physica A **388**, 3391 (2009).
[35] S. K. Dadzie, J. M. Reese, and C. R. McInnes, Physica A **387**, 6079 (2008).
[36] S. K. Dadzie and J. M. Reese, arXiv:1202.3169.
[37] S. K. Dadzie and J. M. Reese, Phys. Rev. E **85**, 041202 (2012).
[38] I. A. Graur, J. G. Meolans, and D. E. Zeitoun, Microfluid Nanofluid **2**, 64 (2006).
[39] W. Mandell and J. West, in *Proceedings of the Physical Society of London*, Vol. 37 (Physical Society of London, London, 1924), pp. 20–41.
[40] H. Peterson, Technical report, Report-Riso-224, Danish Atomic Energy Commision Research Establishment Riso, 1970 (unpublished).
[41] G. A. Bird, *Molecular Gas Dynamics and the Direct Simulation of Gas Flows*, Oxford Engineering Science Series (Clarendon press, Oxford, 1994).
[42] C. J. Greenshields and J. M. Reese, J. Fluid Mech. **580**, 407 (2007).
[43] A. V. Itterbeek and O. V. Paemel, Physica **7**, 273 (1940).
[44] H. Shimotake and G. Thodos, AIChE J. **4**, 257 (1958).
[45] H. C. Öttinger, H. L. Struchtrup, and M. Liu, Phys. Rev. E **80**, 056303 (2009).